IEEE Photonics Journal
An IEEE Photonics Society Publication

Open Access

A Simple Numerical Modeling of the Effect of the Incoherent Thick Substrate in Thin-Film Solar Cells Based on the Equispaced Thickness Method

Volume 8, Number 5, October 2016

Kyungnam Kang
Sanghwa Lee
Jungho Kim, *Member, IEEE*
Sungchul Kim
Younho Han
Seungin Baek

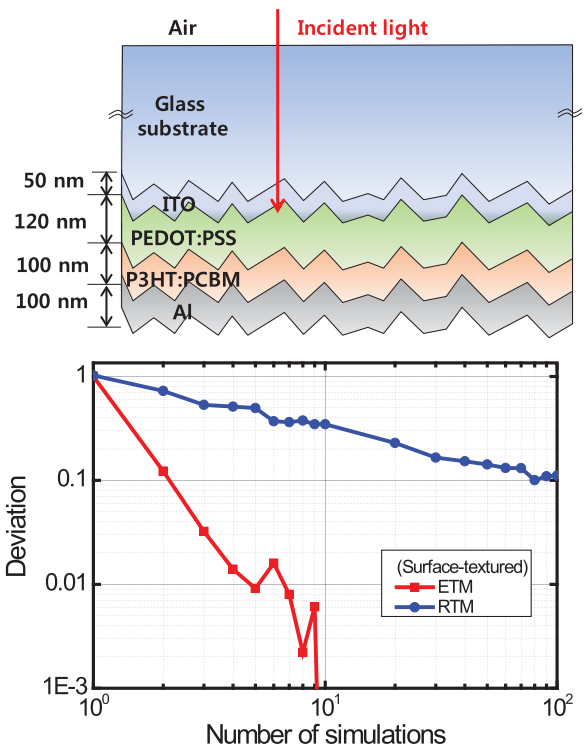

DOI: 10.1109/JPHOT.2016.2614098
1943-0655

A Simple Numerical Modeling of the Effect of the Incoherent Thick Substrate in Thin-Film Solar Cells Based on the Equispaced Thickness Method

Kyungnam Kang,[1] Sanghwa Lee,[1] Jungho Kim,[1] *Member, IEEE*, Sungchul Kim,[2] Younho Han,[3] and Seungin Baek[3]

[1]Department of Information Display and Advanced Display Research Center, Kyung Hee University, Seoul 130-701, South Korea
[2]Department of Information and Communications Engineering, Myongji University, Gyeonggi-do 449-728, South Korea
[3]CAE Team, Samsung Display Company, Gyeonggi-do 446-711, South Korea

DOI:10.1109/JPHOT.2016.2614098

Manuscript received July 30, 2016; revised September 23, 2016; accepted September 25, 2016. Date of publication September 27, 2016; date of current version October 19, 2016. This work was supported in part by the Basic Science Research Program through the National Research Foundation of Korea funded by the Ministry of Education under Grant 2013R1A1A2007034; in part by the Human Resources Development program of the Korea Institute of Energy Technology Evaluation and Planning funded by the Korea Government Ministry of Trade, Industry, and Energy under Grant 20154010200830; and in part by the OLED Research Center funded by Samsung Display. Corresponding author: J. Kim (e-mail: junghokim@khu.ac.kr).

Abstract: We propose a simple numerical modeling method to consider the effect of the incoherent thick substrate on the absorption characteristics of thin-film solar cells. In the proposed "equispaced thickness method" (ETM), the incoherent optical characteristics of the thick substrate are modeled by adding an additional thickness that gives an equispaced phase shift to the incoherent substrate and averaging the coherent simulation results over several equispaced thicknesses. The proposed ETM can be used to consider the effect of the incoherent glass substrate without complicated mathematical and computational procedures and is applicable to not only planar but also surface-textured thin-film solar cells. By applying the proposed method to the numerical modeling based on the finite element method (FEM), we calculate the reflectance spectra in planar and surface-textured thin-film solar cells, respectively. The simulation condition of the FEM, such as mesh size, is determined to match the numerical results based on the ETM with the analytical results obtained by the generalized transfer matrix method. For comparison, the reflectance spectra in the same structures are calculated by taking the average over coherent calculation results for a large number of random thicknesses of the incoherent layer. According to the comparison of the calculated statistical deviations from the exact solution between the ETM and the random thickness method, the ETM reduces the number of simulations by at least a factor of 50 with the same accuracy.

Index Terms: Thin-film solar cells, optical model, incoherence.

1. Introduction

Thin-film solar cells have been intensively studied as one of the promising green energy sources due to the possibility of low cost and high efficiency [1]. Thin-film solar cells have been implemented in

various materials such as amorphous silicon, CdTe, Cu(In, Ga)Se_2, and organic compounds [2]–[5]. Most thin-film solar cells consist of multiple thin layers, having the total thickness of less than one micrometer and a thick substrate on the order of one millimeter. In the optical design of thin-film solar cells, optimizing the thickness of each thin-film layer based on the optical interference effect, which enables us to maximize the optical absorption in the active region, is important to obtain the best efficiency [5], [6].

Because the sunlight has a finite coherence length, the optical interference effect begins to disappear when the total thickness of the thin-film layer is larger than the coherence length of the sunlight. The narrow oscillations in the calculated reflection spectrum of a thin-film multilayer, obtained with the assumption of the coherent light, disappeared when the coherence length of the sunlight was considered [7], [8]. Although the incoherent light transmission in the thick glass substrate did not contribute to the optical interference effect, it increased the light reflectance from the air and decreased the efficiency of thin-film organic solar cells [9], [10]. According to the theoretical calculation, the coherence length of the sunlight was estimated to be 0.6 μm [11]. Thus, thin-film solar cells should be optically modeled as a mixed coherent-incoherent system, where multiple thin layers are treated as optically coherent and the thick substrate is considered as incoherent.

In thin-film optics, the generalized transfer matrix method (GTMM) was widely used to calculate the reflectance and transmittance of mixed coherent-incoherent multilayer systems [12], [13]. The propagation behavior of the electric field intensity in incoherent layers was separately described by matrix formalism similar to the transfer matrix method (TMM) used in coherent layers. In another approach of so-called "random phase method" (RPM), all the layers were treated coherently based on the TMM and the incoherence was introduced by adding a random phase shift in the selected incoherent layer [14]. The transmittance of the mixed coherent-incoherent multilayer was calculated by averaging the calculated transmittances with different values of random phase shifts. Recently, an improved averaging procedure of so-called "equidistance phase method" (EPM) was proposed by means of using only a few equidistant phase shifts in the selected incoherent layer [15]. Because the internal quantum efficiency, determined by the charge transfer and collection processes, depends on the thickness of the active layer or the morphology of the electrode, the spatial distributions of the optical absorption inside a thin-film multilayer affect the external quantum efficiency of solar cells [16], [17]. However, it has not yet been investigated whether the previous averaging procedures of the RPM and the EPM can be applied to the calculation of the spatial distributions of the optical absorption inside a mixed coherent-incoherent multilayer such as a thin-film solar cell.

Non-planar [18] or surface-textured structures [19] are essential to improve the efficiency of solar cells. Various numerical simulation methods such as the rigorous coupled wave analysis (RCWA) [8], [20], the finite element method (FEM) [18], [21], and the finite-difference time-domain (FDTD) [22]–[26] can be used to calculate the optical characteristics of non-planar or surface-textured solar cells. Because the numerical simulation methods directly solve the Maxwell's equations, they require an additional procedure to treat the incoherent light propagation in mixed coherent-incoherent structures. In the case of so-called spectral averaging method, the effect of a partially coherent light was considered by averaging the coherent spectral response with the appropriate weighting function [8], [20]. The first-principle calculation of solar cell efficiency under incoherent illumination was performed through the convolution between the coherent spectral response and the incoherence spectral function [27]. Another method of so-called "one-pass coherent calculation" replaced the rough diffuser structure with a superposition of relaunched plane waves to numerically model combined coherent and incoherent scattering [28]. However, these methods required additional mathematically-complicated processes, which greatly increased the computation complexity and time. In addition, the above-mentioned numerical methods could not effectively treat the large mismatch in scale between the mm-thick incoherent substrate and the μm-thick coherent multiple thin layers, which posed huge computational complexity especially for the FEM and the FDTD. Although a scattering matrix domain decomposition algorithm was proposed to efficiently calculate the incoherent effect of the thick substrate in the FEM, it also required very complicated mathematical and computational procedures [29].

In thin-film optics, Prentice calculated the effect of the incoherent layer on the light absorption in thin-film structures by taking the average over coherent results for a large number of thicknesses of the incoherent layer [30]. This so-called "random thickness method" (RTM) can be considered as the conversion of a random phase shift in the RPM into the equivalent random phase thickness. If the RTM is applied to the numerical modeling of solar cells in the combination of the FEM or the FDTD, it will take very long computation time because a large number of the numerical simulations with different thicknesses are required to obtain the acceptable calculation accuracy. Recently, Campa *et al.* introduced the phase elimination method (PEM) for incoherent propagation of light in the thick substrate. In the PEM, only two coherent simulations with the appropriate thickness difference in the incoherent layer were averaged to eliminate the interference term in the incoherent layer [31]. However, the PEM required very tiny mesh size to avoid discretization phase error, which will increase the computation time [31]. In addition, the PEM ignored the high-order multiple reflection terms in the incoherent layer, which would induce additional computation error.

In this paper, we present a simple method to calculate the optical absorption characteristics of the mixed coherent-incoherent systems in the numerical methods by introducing the "equispaced phase thickness" in the incoherent layer. In the proposed equispaced thickness method (ETM), the value of an equidistant phase shift in the thin-film optics is converted into the equivalent equispaced thickness in the numerical methods and the coherent numerical results are averaged over the equispaced thicknesses. By applying the proposed method to the FEM, we calculate the reflectance spectra in the planar and surface-textured thin-film solar cells. The simulation condition of the FEM such as mesh size is investigated to match the proposed numerical results with the analytical results obtained by the GTMM. For comparison, the reflectance spectra in the same structures are calculated by means of the RTM in the planar thin-film solar cell. The ETM gives the same accuracy as the RTM, but reduces the number of simulations at least by a factor of 50. The calculation results verify that the proposed ETM gives the acceptable accuracy without long computation complexity in the numerical modeling of mixed coherent-incoherent thin-film solar cells.

2. Theory

Fig. 1 shows a schematic diagram of the mixed coherent and incoherent multilayers, which are sandwiched between semi-infinite transparent ambient (usually air) on the left ($j = 0$) and on the right ($j = m + 1$). Each layer has a thickness of d_j and a complex refractive index of $\tilde{n}_j = n_j + \kappa_j$, where n_j and κ_j are the refractive index and the extinction coefficient, respectively. It is assumed that the light incoming from the ambient on the left ($j = 0$) is perpendicularly incident to the multilayer. However, the mathematical proof given here can be easily expanded to the oblique incidence of the incoming light by means of $\tilde{n}_j \cos\phi_j$, where is ϕ_j is a complex refraction angle [32]. In thin-film solar cells, the first layer ($j = 1$) usually consists of a thick transparent substrate such as glass, which can be considered as optically incoherent with no absorption.

We assume the mixed coherent and incoherent multilayer to be isotropic and homogeneous with plane and parallel interfaces. The orientation of the electromagnetic field consists of *s* and *p* polarizations that are orthogonal to (*x* component) or parallel to (*y* component) the incident plane, respectively. When the light propagating from the left to the right is assumed to have a positive direction, the wave in the positive (negative) direction is represented by the $+(-)$ superscripts. In the TMM, the optical behavior in the multilayer is described by the interface matrix (***I***) and the layer matrix (***L***) [6, 9]. The electric field amplitudes at the interface between j th and k th layers are given by

$$\begin{bmatrix} E_{jR}^{+} \\ E_{jR}^{-} \end{bmatrix} = \mathbf{I}_{jk} \begin{bmatrix} E_{kL}^{+} \\ E_{kL}^{-} \end{bmatrix} = \frac{1}{t_{jk}} \begin{bmatrix} 1 & r_{jk} \\ r_{jk} & 1 \end{bmatrix} \begin{bmatrix} E_{kL}^{+} \\ E_{kL}^{-} \end{bmatrix} \tag{1}$$

where r_{jk} and t_{jk} represent the complex Fresnel reflection and transmission coefficients at the interface from the j th to k th layer, respectively. The electric field amplitudes at left and right

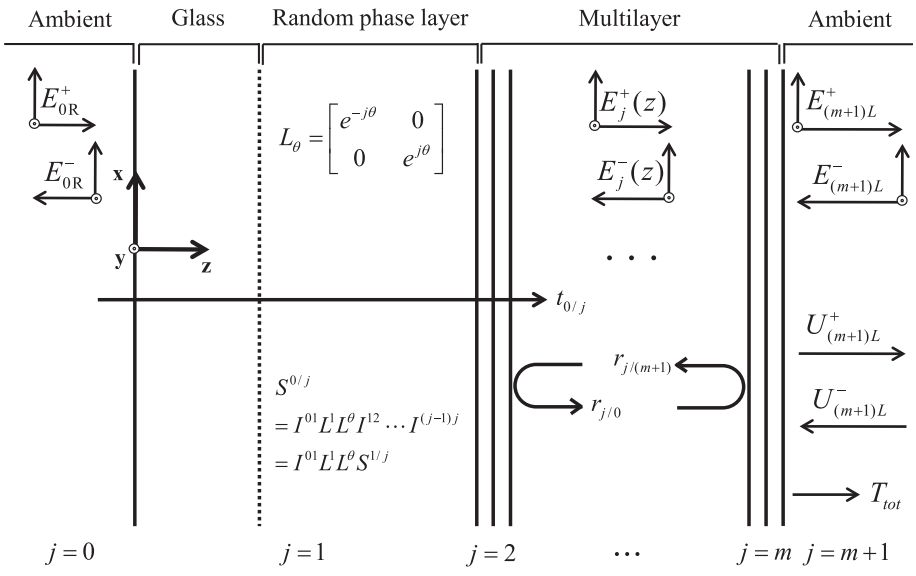

Fig. 1. Schematic diagram of thin-film solar cells with forward- and backward-propagating electric field amplitudes (*E*). There are mixed coherent and incoherent multilayers between semi-infinite transparent ambient (usually air). The $j = 1$ layer is designated to be the incoherent glass with the random phase layer. The other layers are treated as coherent.

boundaries of the j th layer are described by

$$\begin{bmatrix} E^+_{jR} \\ E^-_{jR} \end{bmatrix} = \mathbf{L}_j \begin{bmatrix} E^+_{jL} \\ E^-_{jL} \end{bmatrix} = \begin{bmatrix} e^{-i\beta_j d_j} & 0 \\ 0 & e^{j\beta_j d_j} \end{bmatrix} \begin{bmatrix} E^+_{jL} \\ E^-_{jL} \end{bmatrix} \tag{2}$$

where $\beta_j = (2\pi/\lambda)\cdot\tilde{n}_j$ indicates the propagation constant in the j th layer, and λ is the wavelength of light in free space. In the incoherent layer (j = 1), the additional layer matrix for the random phase shift is given by

$$\mathbf{L}_\theta = \begin{bmatrix} e^{-i\theta} & 0 \\ 0 & e^{j\theta} \end{bmatrix} \tag{3}$$

where θ is a random phase shift between 0 and π [14]. The electric field amplitude between the incoherent layer (j = 1) and the j th layer is related by the system transfer matrix $\mathbf{S}_{1j}$ as follows:

$$\begin{bmatrix} E^+_{1R} \\ E^-_{1R} \end{bmatrix} = \mathbf{I}_{12}\mathbf{L}_2\mathbf{I}_{23}\cdots\mathbf{L}_{j-1}\mathbf{I}_{(j-1)j} \begin{bmatrix} E^+_{jL} \\ E^-_{jL} \end{bmatrix} = \begin{bmatrix} S^{11}_{1j} & S^{12}_{1j} \\ S^{21}_{1j} & S^{22}_{1j} \end{bmatrix} \begin{bmatrix} E^+_{jL} \\ E^-_{jL} \end{bmatrix}. \tag{4}$$

The electric field amplitudes in the ambient (j = 0) and at the right-hand boundary of the incoherent layer (j = 1) are related by

$$\begin{bmatrix} E^+_{0R} \\ E^-_{0R} \end{bmatrix} = \mathbf{I}_{01}\mathbf{L}_1\mathbf{L}_\theta \begin{bmatrix} E^+_{1R} \\ E^-_{1R} \end{bmatrix} = \frac{1}{t_{01}} \begin{bmatrix} 1 & r_{01} \\ r_{01} & 1 \end{bmatrix} \begin{bmatrix} e^{-i\beta_1 d_1} & 0 \\ 0 & e^{j\beta_1 d_1} \end{bmatrix} \begin{bmatrix} e^{-i\theta} & 0 \\ 0 & e^{i\theta} \end{bmatrix} \begin{bmatrix} E^+_{1R} \\ E^-_{1R} \end{bmatrix} \tag{5}$$

where the random phase value is added in the incoherent layer. The system transfer matrix between the ambient (j = 0) and the j th layer $\mathbf{S}_{0j}$ is expressed as

$$\begin{aligned} \mathbf{S}_{0j} &= \mathbf{I}_{01}\mathbf{L}_1\mathbf{L}_\theta\mathbf{S}_{1j} = \frac{1}{t_{01}} \begin{bmatrix} e^{-i(\beta_1 d_1+\theta)} & r_{01}e^{j(\beta_1 d_1+\theta)} \\ r_{01}e^{-i(\beta_1 d_1+\theta)} & e^{j(\beta_1 d_1+\theta)} \end{bmatrix} \begin{bmatrix} S^{11}_{1j} & S^{12}_{1j} \\ S^{21}_{1j} & S^{22}_{1j} \end{bmatrix} \\ &= \frac{1}{t_{01}} \begin{bmatrix} S^{11}_{1j}e^{-i(\beta_1 d_1+\theta)} + r_{01}S^{21}_{1j}e^{j(\beta_1 d_1+\theta)} & S^{12}_{1j}e^{-i(\beta_1 d_1+\theta)} + r_{01}S^{22}_{1j}e^{j(\beta_1 d_1+\theta)} \\ r_{01}S^{11}_{1j}e^{-i(\beta_1 d_1+\theta)} + S^{21}_{1j}e^{j(\beta_1 d_1+\theta)} & r_{01}S^{12}_{1j}e^{-i(\beta_1 d_1+\theta)} + S^{22}_{1j}e^{j(\beta_1 d_1+\theta)} \end{bmatrix}. \end{aligned} \tag{6}$$

The front-transmission and front-reflection coefficients from the layer 0 to j are written as

$$\mathrm{t}_{0j}(\theta) = \frac{E_{jL}^{+}}{E_{0R}^{+}} = \frac{1}{S_{0j}^{11}} \tag{7}$$

$$\mathrm{r}_{0j}(\theta) = \frac{E_{0R}^{-}}{E_{0R}^{+}} = \frac{S_{0j}^{21}}{S_{0j}^{11}}. \tag{8}$$

Finally, the electric field intensity within the j th layer is given by

$$\begin{aligned} \left|\mathrm{E}_j(z,\theta)\right|^2 &= \left|t_j^{+}\right|^2 \left|e^{j\beta_j z} + r_{j(m+1)}e^{-i\beta_j z}\right|^2 \left|\mathrm{E}_{0R}^{+}\right|^2 \\ &= \left(\frac{t_{0j}}{1 + r_{0j}r_{j(m+1)}e^{2i\beta_j d_j}} \cdot \frac{t_{0j}^{*}}{1 + r_{0j}^{*}r_{j(m+1)}^{*}e^{-2i\beta_j d_j}}\right) \left|e^{j\beta_j z} + r_{j(m+1)}e^{-i\beta_j z}\right|^2 \left|\mathrm{E}_{0R}^{+}\right|^2 \end{aligned} \tag{9}$$

where t_j^{+} indicates the forward-propagating internal transfer coefficient, and the relation of $r_{0j} = -r_{j0}$ is used [6], [9].

According to the RPM, the electric field intensity within the j-th layer can be obtained by averaging all the calculated electric field intensities over random phase shifts, which is expressed as

$$\left|\mathrm{E}_j(z)\right|^2 = \frac{1}{N}\sum_{r=1}^{N}\left|\mathrm{E}_j(z,\theta_r)\right|^2. \tag{10}$$

Here, N represents the number of coherent simulations with different random phase shifts of $0 \le \theta_r \le \pi$ [14]. The calculated electric field intensities in the mixed coherent-incoherent multilayer become more accurate as the number N becomes larger. In the case of the EPM, the number of coherent simulations can be greatly reduced without the loss of accuracy by selecting equidistant phase values [15]. If five equidistant phase shifts are used in the selected incoherent layer, we can set $\theta_1 = 0$, $\theta_2 = \pi/5$, $\theta_3 = 2\pi/5$, $\theta_4 = 3\pi/5$, and $\theta_5 = 4\pi/5$. Then, the electric field intensity inside the j-th layer can be obtained by

$$\left|\mathrm{E}_j(z)\right|^2 = \frac{1}{5}\sum_{e=1}^{5}\left|\mathrm{E}_j(z,\theta_e)\right|^2. \tag{11}$$

Correspondingly, the spatial distribution of the light absorption within the j-th layer is given by [6, 9]

$$Q_j(z) = \frac{1}{2}c\varepsilon_0 n_j \alpha_j \left|\mathrm{E}_j(z)\right|^2 \tag{12}$$

where c is the speed of light in free space, ε_0 is the electric permittivity in free space, and $\alpha_j = 4\pi\kappa_j/\lambda$ is the absorption coefficient. Finally, the absorbance at the j th layer ($d_{j-1} \le z \le d_j$) can be obtained by

$$A_j = \frac{1}{P_0}\int_{d_{j-1}}^{d_j} Q_j(z)dz, \tag{13}$$

where P_0 is the optical power of the sunlight incoming from the ambient on the left (j = 0). The incident sunlight is totally absorbed in the active region or metal electrode of the thin-film solar cell without reaching the ambient on the right (j = m + 1). Thus, the total reflectance of the thin-film solar cell in Fig. 1 can be expressed as

$$R_{tot} = 1 - \sum_{j=1}^{m} A_j. \tag{14}$$

In the numerical simulation, a discrete value of the random phase shift θ_r cannot be directly assigned to the physical geometry. In this case, the value of the random phase shift can be converted into the additional equivalent random thickness in the numerical simulation. If the incoherent layer

in Fig. 1 is transparent, the propagation constant is a real value of $\beta_1 = (2\pi/\lambda) \cdot n_1$. Hence, the random thickness of d_r is determined by the random phase shift of θ_r as follows:

$$d_r = \frac{\lambda_r}{2n_1}\frac{\theta_r}{\pi}, \quad 0 \le \theta_r \le \pi. \tag{15}$$

This equation indicates the conversion relation between a random phase shift in the RPM and a random thickness in the RTM. In the case of the ETM, the equispaced phase thickness is given by

$$d_x = \frac{\lambda}{2n_1}\frac{(q-1)}{X}, \quad q = 1, 2, \cdots, (X-1), X \tag{16}$$

where X is the number of the equispaced thickness. If the number of the equispaced thickness is two, the corresponding additional thicknesses are

$$d_1 = 0, d_2 = \frac{\lambda}{4n_1}, \tag{17}$$

which is exactly the same thicknesses used in the PEM [31]. When five equispaced thicknesses are used in the ETM, the additional thicknesses are

$$d_1 = 0, d_2 = \frac{\lambda}{10n_1}, d_3 = \frac{2\lambda}{10n_1}, d_4 = \frac{3\lambda}{10n_1}, d_5 = \frac{4\lambda}{10n_1}. \tag{18}$$

Here, the additional equispaced thicknesses are varied with respect to the wavelength of light. However, this does not affect the complexity and accuracy of the numerical simulation.

Because the "equidistance phase" in the EPM and the "equispaced phase thickness" in the ETM can be directly converted by (15), two methods are mathematically equivalent. However, the ETM has the advantage over the EPM in that the ETM can be applied to both planar and surface-textured structures. In the case of the EPM, discrete values of equidistant phase shifts are averaged to consider the effect of the incoherent thick glass substrate in the planar thin-film structure [15]. However, a discrete value of equidistant phase shift cannot be directly assigned to the physical geometry in the numerical modeling based on the FEM or the FDTD. Thus, the EPM has a limitation that it cannot be applied to non-planar or surface-textured structures, where only numerical modeling method can be used. In contrast, the equispaced phase thickness in the ETM can be assigned to the physical geometry to consider the effect of the incoherent thick glass substrate in both planar and surface-textured structures. Because both the FEM and the FDTD numerically solve the Maxwell's equations within spatially discretized meshes or grids, the ETM can be applied to the FDTD as well as the FEM. In this paper, we show the calculated optical characteristics of thin-film solar cells by applying the proposed ETM to the FEM.

3. Simulation Results

3.1. Planar Thin-Film Solar Cells

Fig. 2(a) shows a device structure of the planar thin-film organic solar cell (OSC), which is composed of glass/indium tin oxide (ITO)/poly(3,4-ethylenedioxythiophene):poly(styrene sulfonate) (PEDOT:PSS)/poly(3-hexylthiophene):[6,6]-phenyl C61-butyric acid methyl ester (P3HT:PCBM)/Al (aluminum). Fig. 2(b) shows the complex refractive index spectra that are measured by the spectroscopic ellipsometry [32]. The values of the corresponding thickness and the complex refractive index ($\lambda = 550$ nm) in each layer are designated in Fig. 2(a). The glass substrate with the thickness of 1 mm is optically modeled as an incoherent layer because its thickness is much larger than the coherence length of the sunlight (0.6 μm) [11]. The remaining total thickness of the multilayer in-between the ITO and the Al layers is 0.37 μm and considered as the coherent multilayer.

The planar thin-film OSC is numerically modeled based on the two-dimensional FEM, which is performed by the commercial software COMSOL MULTIPHYSICS [33]. In the FEM calculation, the planar thin-film OSC is divided into small meshes, where the Maxwell equation is numerically solved with appropriate boundary conditions. The periodic boundary condition is applied at the left- and

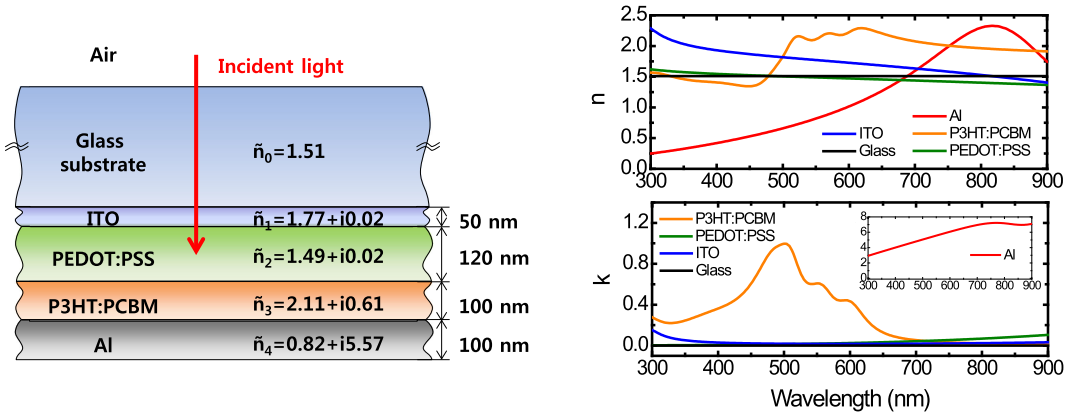

(a) (b)

Fig. 2. (a) Device structure of the planar thin-film OSC. (b) Complex refractive index spectra of the materials measured by the spectroscopic ellipsometry.

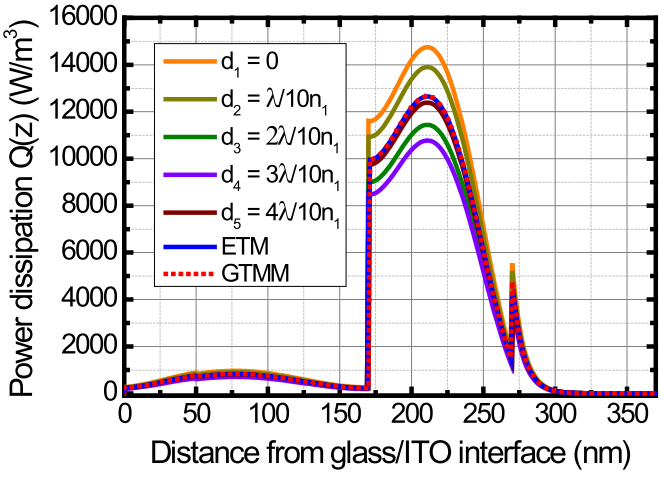

Fig. 3. Calculated spatial distribution of the power dissipation Q(z) depending on the five equispaced phase thicknesses of d_1, d_2, d_3, d_4, and d_5 in incoherent glass layer. To consider the effect of the incoherent glass substrate, the calculation result based on the ETM is obtained by averaging the five calculation results. The numerical result obtained by the ETM is well matched with the analytical result based on the GTMM, which is considered as the exact solution in the planar thin-film solar cell.

the right-hand boundaries while the scattering boundary condition is used for the top and the bottom boundaries. Because the thick glass substrate works as an incoherent layer, the additional glass thicknesses are chosen based on (15) and (16) for the RTM and the ETM, respectively. In addition, the initial thickness of the thick glass substrate needs not to be taken as an actual value on the order of millimeter because the glass substrate has no absorption coefficient [31]. In this calculation, we choose the initial glass thickness as 1 μm, which is two or three times larger than the maximal phase thickness of $d = \lambda/2n_1$.

At first, the spatial distribution of the power dissipation Q(z) is calculated with respect to different phase thickness of the incoherent glass substrate. Fig. 3 shows the calculated spatial distributions of the power dissipation at the wavelength of 550 nm when five equispaced thicknesses are used in the ETM. The reason why five equispaced thicknesses are used in the ETM will be explained in Fig. 5. As the additional thickness in the incoherent glass substrate increases from $d_1 = 0$ to $d_5 = 2\lambda/5n_1$, the overall magnitude of Q(z) is varied while the overall shape of Q(z) is unchanged.

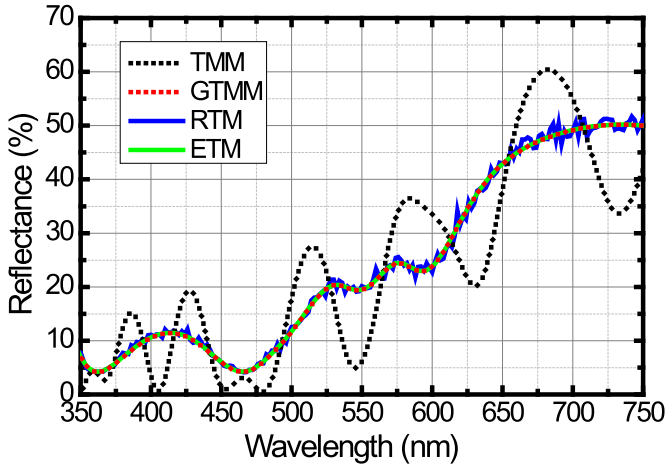

Fig. 4. Comparison of the calculated reflectance spectra of the planar thin-film OSC among the TMM, the GTMM, the RTM, and the ETM. In the numerical calculations, five equispaced phase thicknesses and 100 random phase thicknesses are averaged in the ETM and the RTM, respectively. Except for the TMM, the other three methods nearly give the same results.

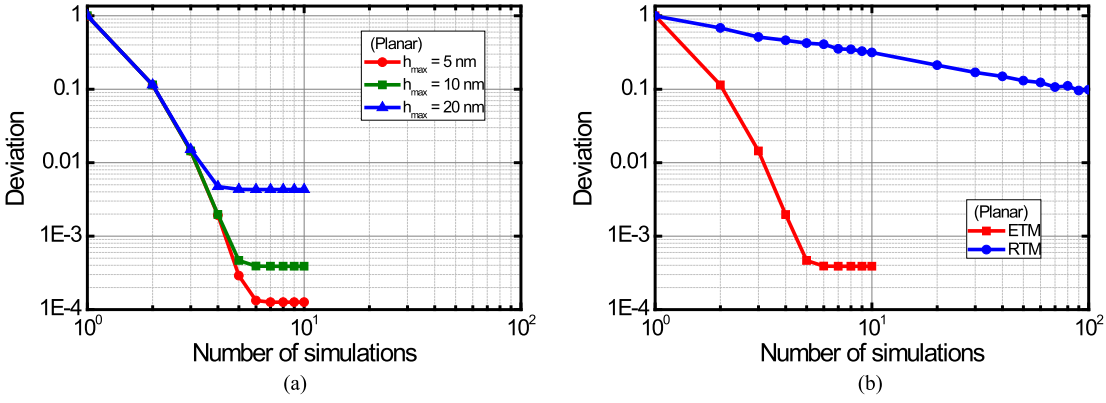

Fig. 5. (a) Deviation from the exact solution as a function of the number of the FEM simulations with different phase thickness when the maximal mesh size in the FEM calculation is set to be 5, 10, and 20 nm. As the number of equispaced thickness in the ETM increases, the deviation is reduced and converges to a certain value of the discretization error for each maximal mesh size. (b) Deviation from the exact solution depending on the number of the FEM simulations with different phase thickness for the ETM and the RTM. The deviation in the ETM decreases faster than that in the RTM as the number of the FEM simulations with different phase thicknesses become larger.

After five coherent calculation results of Q(z) with different additional thickness are averaged, we obtain the ETM-based Q(z) to consider the effect of the incoherent glass substrate. For comparison, Q(z) is also calculated based on the GTMM, which is considered as the exact analytical solution in the planar thin-film solar cell with the incoherent effect of the glass substrate considered. The numerical result based on the ETM is well matched with the analytical result based on the GTMM, which verifies the accuracy of the ETM in the numerical modeling of mixed coherent-incoherent multilayer.

Fig. 4 shows the calculated reflectance spectra of the planar thin-film OSC obtained by the four calculation methods, which correspond to the TMM, the GTMM, the RTM, and the ETM. In the numerical calculations, five equispaced phase thicknesses and 100 random phase thicknesses are averaged in the ETM and the RTM, respectively. The calculation result based on the TMM has a reflection ripple because the 1-μm-thick glass substrate in Fig. 2(a) is modeled as a coherent

layer. However, this reflection ripple disappears in the calculation results obtained by the other three methods. The reflectance calculated by the ETM and the RTM almost converges to the calculation result based on the GTMM. However, the reflectance obtained by the RTM has some deviations from that calculated by the GTMM in the long wavelength range. A larger number of random phase thicknesses to be averaged are required to further reduce the calculation deviation of the RTM.

To verify the accuracy of the proposed ETM, the statistical deviation is calculated in the planar thin-film OSC. The deviations in the ETM and the RTM are defined as

$$\sigma_{ETM(RTM)}(r) = \sqrt{\frac{\left(\sum_{g=1}^{G}\left(R^{r}_{ETM(RTM)}(g) - R_{GTMM}(g)\right)^{2}\right)/G}{\left(\sum_{g=1}^{G}\left(R^{1}_{ETM}(g) - R_{GTMM}(g)\right)^{2}\right)/G}} \tag{19}$$

where G is the total number of discrete wavelengths used in the FEM calculation, and r is the number of FEM simulations used in the average procedure. The terms $R^{r}_{ETM}(g)$ and $R^{r}_{RTM}(g)$ are the optical reflectance at the g-th wavelength when r simulations are averaged in the ETM or the RTM. The term $R_{GTMM}(g)$ is the optical reflectance at the g-th wavelength in the GTMM, which is set to be the value of the exact solution.

Fig. 5(a) shows the deviations from the exact solution as a function of the number of the FEM simulations with different phase thickness when the maximal mesh size in the FEM calculation is set to be 5, 10, and 20 nm. As the number of the equispaced thickness in the ETM increases, the deviation is reduced and converges to a certain value, which corresponds to a discretization phase error for each maximal mesh size. The smaller mesh size acquires the lower deviation. We set the maximal mesh size to be 10 nm in this calculation by optimizing the simulation condition between calculation time and accuracy. Fig. 5(b) shows the deviations from the exact solution depending on the number of the FEM simulations with different phase thickness, which is determined based on the ETM and the RTM. Because the deviation is normalized for the single coherent simulation with the glass thickness of $d_1 = 0$, the deviation of the ETM has a unity value when the number of FEM simulations is one. On the other hand, the deviation of the RTM is not one in the first simulation because the first random thickness could not be chosen as $d_1 = 0$. In the case of the ETM, the deviations begin to be less than 0.1% in the planar thin-film OSC as the number of FEM simulations with corresponding equispaced thicknesses is larger than five. However, the deviation for the RTM is reduced so slowly that the deviation only decreases down to 10% although 100 FEM simulations with corresponding random thicknesses are averaged. On the other hand, the ETM only needs two FEM simulations to reach the deviation down to 10%. Thus, the ETM gives the same accuracy as the RTM, but reduces the number of simulations at least by a factor of 50 to numerically calculate the effect of the incoherent glass substrate in thin-film solar cells.

3.2. Surface-Textured Thin-Film Solar Cells

Fig. 6(a) shows a device structure of the surface-textured thin-film OSC, where the interface of the multilayer is randomly textured to enhance light absorption caused by the scattering effect [19]. The layer thickness and corresponding complex refractive index are also identical to those of the planar thin-film OSC in Fig. 2. The 2-D FEM is used in the numerical modeling together with the same boundary conditions used for the planar thin-film OSC. Fig. 6(b) shows the calculated reflectance spectra in the surface-textured thin-film OSC without and with the effect of the incoherent glass substrate considered. Because the glass substrate is considered as perfectly coherent, the calculation result marked in the black dotted line has the reflectance ripples. The effect of the incoherent glass substrate is considered based on the ETM, where ten FEM simulations with the corresponding equispaced thicknesses of the glass substrate are averaged. The ripple of the reflectance spectrum disappears when the ETM is applied to the surface-textured thin-film OSC. In addition, the spectral response of the reflectance in the surface-textured thin-film OSC is lower than that in the planar thin-film OSC, which is designated in the red dotted line. This calculation

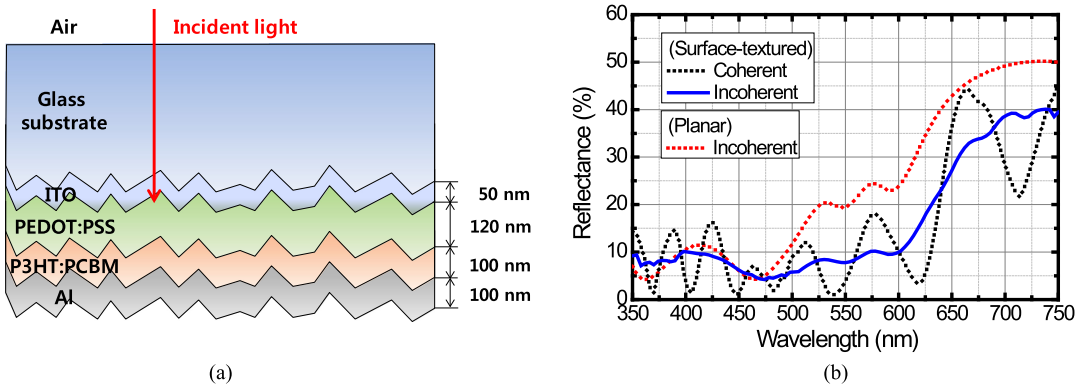

Fig. 6. (a) Device structure of the surface-textured thin-film OSC. (b) Calculated reflectance spectra of the surface-textured OSC without and with the effect of the incoherent glass substrate considered. The red dotted line indicates the calculated reflectance spectrum of the planar thin-film OSC based on the ETM.

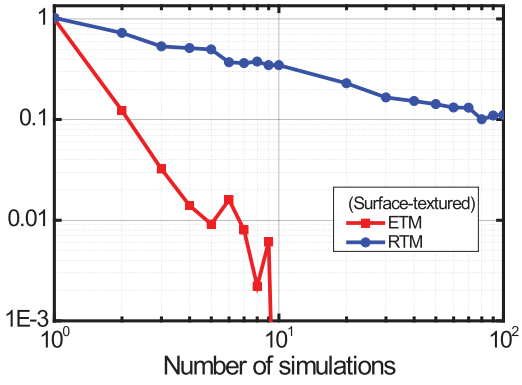

Fig. 7. Deviation from the exact solution depending on the number of the FEM simulations with different additional phase thickness in the surface-textured thin-film OSC. The exact solution of the reflectance spectrum is set to be an average value over ten FEM simulations in the ETM. The deviation in the ETM decreases faster than that in the RTM as the number of the FEM simulations with different phase thicknesses increases.

result demonstrates the enhancement of the absorption in the surface-textured OSC caused by the scattering effect in the randomly-textured structure.

To investigate the accuracy of the proposed ETM, the statistical deviation is also calculated in the surface-textured thin-film OSC. In the case of the surface-textured thin-film OSC, there is no analytically exact solution to the spatial distribution of light absorption at each mesh point when the effect of the incoherent glass substrate is considered. Referring to the previous work [15], we set the exact solution of the reflectance to be an average value based on ten simulations for the ETM. Therefore, the deviations of the ETM and the RTM are defined as

$$\sigma_{ETM(RTM)}(r) = \sqrt{\frac{\left(\sum_{g=1}^{G}\left(R^{r}_{ETM(RTM)}(g) - R^{10}_{ETM}(g)\right)^2\right)/G}{\left(\sum_{g=1}^{G}\left(R^{1}_{ETM}(g) - R^{10}_{ETM}(g)\right)^2\right)/G}} \tag{20}$$

where $R^{10}_{ETM}(g)$ is the optical reflectance in the ETM with ten FEM simulations averaged and is assumed to the exact solution.

Fig. 7 shows the deviations from the exact solution depending on the number of the FEM simulations with different additional thickness in the surface-textured thin-film OSC. When the phase

thickness is determined based on the ETM, the deviations become less than 1% as the number of FEM simulations with corresponding equispaced thicknesses is larger than seven. On the other hand, the deviation for the RTM decreases so slowly that the deviation only decreases down to 10%, although 100 coherent FEM simulations with corresponding random thicknesses are averaged. The calculated deviations in Fig. 7 show a similar behavior to those in planar thin-film solar cells [15], which verifies that the proposed ETM is also applicable to the surface-textured thin-film solar cells and can provide the acceptable accuracy without long computation complexity and time. In Fig. 7, the deviation for the ETM has local peaks when six and nine simulations are averaged in the surface-textured thin-film OSC. This will be ascribed to the fact that an arbitrarily textured structure can affect a certain initial phase of light and increase the deviation from the exact solution. If another arbitrarily textured surface is used for the deviation calculation, the local peak will not be observed. In reality, many sets of the FEM simulation with different surface texturing need to be performed to simulate randomly-surface-textured OSCs. In that case, the unwanted peak can be eliminated in the simulation of randomly surface-textured OSCs by averaging ETM-based calculation results over many arbitrarily textured surfaces.

4. Conclusion

We presented a simple numerical modeling method to include the effect of the incoherent thick glass substrate on the optical characteristics of thin-film solar cells. In the proposed ETM, the effect of the incoherent glass substrate was optically modeled by averaging the coherent simulation results over the additional equispaced thicknesses of the incoherent layer. In contrast to the thin-film-based analytical methods of the GTMM and the EPM, the ETM was applicable to surface-textured structures, where only numerical modeling methods such as the FEM and the FDTD could be used. By applying the proposed method to both planar and surface-textured thin-film solar cells, we calculated the reflectance spectra based on the FEM. In the case of the planar thin-film solar cell, the calculation result based on the ETM was well matched with the analytical result obtained by the GTMM. For comparison, the reflectance spectra in the same structures were also numerically calculated based on the RTM, where a large number of random thicknesses was used in the incoherent layer. The statistical deviations from the exact solution were calculated to investigate the simulation accuracy and the computation time between the ETM and the RTM. The ETM provided the same accuracy as the RTM but reduced the number of simulations at least by a factor of 50 in both planar and surface-textured thin-film solar cells. We demonstrate that the proposed ETM gives the acceptable accuracy without long computation complexity and time to consider the effect of the incoherent thick glass substrate in the numerical modeling of thin-film solar cells. We expect that the proposed ETM helps to design more efficient thin-film solar cells, considering the effect of the incoherent thick glass substrate with various light trapping structures.

References

[1] M. A. Green, K. Emery, Y. Hishikawa, W. Warta, and E. D. Dunlop, "Solar cell efficiency tables (version 39)," *Prog. Photovolt. Res. Appl.*, vol. 20, no. 1, pp. 12–20, Jan. 2012.
[2] M. A. Green, "Silicon photovoltaic modules: a brief history of the first 50 years," *Prog. Photovolt. Res. App.*, vol. 13, no. 5, pp. 447–455, Aug. 2005.
[3] J. Britt and C. Ferekides, "Thin-film CdS/CdTe solar cell with 15.8% efficiency," *Appl. Phys. Lett.*, vol. 62, no. 22, Mar. 1993, Art. no. 109629.
[4] I. Repins *et al.*, "19.9%-efficient ZnO/CdS/CuInGaSe2 solar cell with 81.2% fill factor," *Prog. Photovolt. Res. Appl.*, vol. 16, no. 3, pp. 235–239, May 2008.
[5] P. Peumans, A. Yakimov, and S.R. Forrest, "Small molecular weight organic thin-film photodetectors and solar cells," *J. Appl. Phys.*, vol. 93, no. 7, pp. 3693–3723, Apr. 2003.
[6] L. A. A. Pettersson, L. S. Roman, and O. Inganäs, "Modeling photocurrent action spectra of photovoltaic devices based on organic thin films," *J. Appl. Phys.*, vol. 86, no. 1, pp. 487–496, Feb. 1999.
[7] C. L. Mitsas and D. I. Siapkas, "Generalized matrix method for analysis of coherent and incoherent reflectance and transmittance of multilayer structures with rough surfaces, interfaces, and finite substrates," *Appl. Opt.*, vol. 34, no. 10, pp. 1678–1683, Apr. 1995.

[8] W. Lee, S. Lee, J. Kim, S. Kim, and B. Lee, "A numerical analysis of the effect of partially coherent light in photovoltaic devices considering coherence length," *Opt. Exp.*, vol. 20, no. S6, pp. A941–A953, Oct. 2012.
[9] S. Jung *et al.*, "Optical modeling and analysis of organic solar cells with coherent multilayers and incoherent glass substrate using generalized transfer matrix method," *Jpn. J. Appl. Phys.*, vol. 50, no. 12, Nov. 2011, Art. no. 122301.
[10] K. Kang, S. Lee, and J. Kim, "Effect of an incoherent glass substrate on the absorption efficiency of organic solar cells at oblique incidence analyzed by the transfer matrix method with a glass factor," *Jpn. J. Appl. Phys.*, vol. 52, no. 5, Apr. 2013, Art. no. 052301.
[11] A. Donges, "The coherence length of black-body radiation," *Eur. J. Phys.*, vol. 19, no. 3, pp. 245–249, Feb. 1998.
[12] C. C. Katsidis and D. I. Siapkas, "General transfer-matrix method for optical multilayer systems with coherent, partially coherent, and incoherent interference," *Appl. Opt.*, vol. 41, no. 19, pp. 3978–3987, Jan. 2002.
[13] E. Centurioni, "Generalized matrix method for calculation of internal light energy flux in mixed coherent and incoherent multilayers," *Appl. Opt.*, vol. 44, no. 35, pp. 7532–7539, Jul. 2005.
[14] M. C. Troparevsky, A. S. Sabau, A. R. Lupini, and Z. Zhang, "Transfer-matrix formalism for the calculation of optical response in multilayer systems: from coherent to incoherent interference," *Opt. Exp.*, vol. 18, no. 24, pp. 24715–24721, Nov. 2010.
[15] R. Santbergen, A. H. M. Smets, and M. Zeman, "Optical model for multilayer structures with coherent, partly coherent and incoherent layers," *Opt. Exp.*, vol. 21, no. S2, pp. A262–A267, Feb. 2013.
[16] S. E. Forrest, "The limits to organic photovoltaic cell efficiency," *MRS Bull.*, vol. 30, no. 1, pp. 28–32, Jan. 2005.
[17] G. F. Burkhard, E. T. Hoke, and M. D. McGehee, "Accounting for interference, scattering, and electrode absorption to make accurate internal quantum efficiency measurements in organic and other thin solar cells," *Adv. Mater.*, vol. 22, no. 30, pp. 3293–3297, May 2010.
[18] V. Andersson, K. Tvingstedt, and O. Inganäs, "Optical modeling of a folded organic solar cell," *J. Appl. Phys.*, vol. 103, no. 9, May 2008, Art. no. 094520.
[19] M. Berginski *et al.*, "The effect of front ZnO:Al surface texture and optical transparency on efficient light trapping in silicon thin-film solar cells," *J. Appl. Phys.*, vol. 101, no. 7, Apr. 2007, Art. no. 074903.
[20] S. C. Kim, "Simulation of rough surface of CIGS (CuInGaSe) solar cell by RCWA (rigorous coupled wave analysis) considering the incoherency of light," *J. Opt. Soc. Kor.*, vol. 18, no. 2, pp. 180–183, Apr. 2014.
[21] K. Kang and J. Kim, "Effect of sunlight polarization on the absorption efficiency of V-shaped organic solar cells," *J. Opt. Soc. Kor.*, vol. 18, no. 1, pp. 9–14, Feb. 2014.
[22] S. Mokkapati, F. J. Beck, A. Polman, and K. R. Catchpole, "Designing periodic arrays of metal nanoparticles for light-trapping applications in solar cells," *Appl. Phys. Lett.*, vol. 95, no. 5, Aug. 2009, Art. no. 053115.
[23] M. G. Deceglie, V. E. Ferry, A. P. Alivisatos, and H. A. Atwater, "Design of nanostructured solar cells using coupled optical and electrical modeling," *Nano Lett.*, vol. 12, no. 6, pp. 2894–2900, May 2012.
[24] N. Das, F. F. Masouleh, and H. R. Mashayekhi, "Light absorption and reflection in nanostructured GaAs metal-semiconductor-metal photodetectors," *IEEE Trans. Nanotechnol.*, vol. 13, no. 5, pp. 982–989, Sep. 2014.
[25] F. F. Masouleh, N. Das, and S. M. Rozati, "Optimal subwavelength design for efficient light trapping in central slit of plasmonics-based metal-semiconductor-metal photodetector," *Opt. Quantum Electron.*, vol. 47, no. 6, pp. 1477–1485, Feb. 2015.
[26] F. F. Masouleh, N. Das, and H. R. Mashayekhi, "Comparison of different plasmonic nanograting profiles for quality light absorption in nanostructured metal-semiconductor-metal photodetectors," *Opt. Eng.*, vol. 52, no. 12, Dec. 2013, Art. no. 127101.
[27] M. Sarrazin, A. Herman, and O. Deparis, "First-principle calculation of solar cell efficiency under incoherent illumination," *Opt. Exp.*, vol. 21, no. S4, pp. A616–A630, May 2013.
[28] A. Abass, C. Trompoukis, S. Leyre, M. Burgelman, and B. Maes, "Modeling combined coherent and incoherent scattering structures for light trapping in solar cells," *J. Appl. Phys.*, vol. 114, no. 3, Jul. 2013, Art. no. 033101.
[29] M. Hammerschmidt, "Optical modelling of incoherent substrate light-trapping in silicon thin film multi-junction solar cells with finite elements and domain decomposition," in *Proc. SPIE*, vol. 8980, pp. 898007-1–898007-8, Feb. 2014
[30] J. S. C. Prentice, "Coherent, partially coherent and incoherent light absorption in thin-film multilayer structures," *J. Phys. D: Appl. Phys.*, vol. 33, no. 24, pp. 3139–3145, Oct. 2000.
[31] A. Campa, J. Krc, and M. Topic, "Two approaches for incoherent propagation of light in rigorous numerical simulations," *Prog. Electromagn. Res.*, vol. 137, pp. 187–202, Feb. 2013.
[32] S. Lee *et al.*, "Effect of incidence angle and polarization on the optimized layer structure of organic solar cells," *Sol. Energy Mater. Sol. Cells*, vol. 118, pp. 9–17, Aug. 2013.
[33] Comsol Inc., Burlington, MA, USA. *COMSOL Multiphysics, Version 4.4a*, 2013. [Online]. Available: http://www.comsol.com